*Kovove Mater. 61 2023 59–67*
*DOI: 10.31577/km.2023.1.59*



# Corrosion behavior of CoCrNiAl high entropy alloy and other typical metals in simulated acid rain solution

Xingwu Qiu*, Chunge Liu, Jia Peng, Zhansheng Wang

*Sichuan College of Architectural Technology, Deyang 618000, P. R. China*

Received 12 October 2022, received in revised form 13 January 2023, accepted 13 January 2023

**Abstract**

In order to study the accelerated electrochemical corrosion behavior under simulated acid rain, CoCrNiAl high entropy alloy (HEA) was prepared. The electrochemical performance of CoCrNiAl HEA and other typical metals (Q235 steel, AZ31 magnesium alloy, and 1060 aluminum alloy) in simulated acid rain solution with different pH (3.5, 4.0, 4.5, and 5.0) were studied. The results show that the microstructure of CoCrNiAl HEA is mainly composed of dendrites (DR). The alloy exhibits the diffraction patterns of the disordered A2-bcc phase with the ordered B2-bcc phase. Ni-Al is rich in dendrites, and Cr is rich in interdendritic (ID) regions that consist of the A2/B2. The CoCrNiAl HEA has excellent corrosion resistance in simulated acid rain solution with pH = 3.5, 4.0, 4.5, and 5.0. The self-corrosion current is reduced by 1–2 orders of magnitude compared with other typical metals. The self-corrosion potential is higher than for other typical metals except in a solution with pH = 5. The CoCrNiAl HEA has excellent pitting corrosion resistance. The corrosion resistance of CoCrNiAl HEA is related to the uniformity and compactness of the microstructure, passive surface film, and corrosion resistant elements in the alloy. The dense corrosion products on the surface also play a role in reducing the corrosion rate. The corrosion mechanism of the prepared CoCrNiAl alloy is intergranular corrosion when it comes into contact with a simulated acid rain solution, and then with the extension of time, the corrosion mechanism changes to uniform corrosion.

K e y w o r d s: corrosion performance, high entropy alloy, simulated acid rain, vacuum casting, microstructure

## 1. Introduction

Atmospheric precipitation with a pH of less than 5.60 is called acid rain. Acid rain pollution and environmental acidification are significant environmental problems of common concern worldwide. The acid rain damage is much more significant than that of ordinary rain [1–3]. Acid rain accelerates the corrosion rate of materials, especially metal materials [4–6]; it will invalidate various protective coatings, damage buildings and bridges, and cause severe damage. On the other hand, acid rain washes and collects heavy metal ions into nature through the corrosion and scouring of materials. It also releases metal ions such as aluminum, cadmium, lead, and mercury in the soil and enters the human body through the food chain, such as food and fish, which seriously harms human and biological health. Many investigations and studies have shown that the harmful effects of acid rain on materials and cultural relics, and historic sites have been widespread [7–9].

Multicomponent alloys include medium entropy alloys (MEAs) [10–15] and high entropy alloys (HEAs) [16–19]. HEAs and MEAs have attracted more and more attention from experts and scholars [20–26]. CoCrNi MEA has attracted much attention because of its excellent mechanical properties. B. Gludovatz et al. [27] found that the CrCoNi alloy displays strength-toughness properties that exceed those of all high-entropy and most multi-phase alloys. At room temperature, the alloy shows a tensile strength of almost 1 GPa and a failure strain of ∼70 %. The corrosion behavior of some HEAs and MEAs in various liquids has been investigated. H. Luo et al. [28] stud-

*Corresponding author: e-mail address: qiuxingwu2021@163.com

ied the corrosion resistance and passive film properties of CoCrFeMnNi in 0.1 M $H_2SO_4$ solution compared with the 304 L stainless steel. It is found that the in-situ element-resolved corrosion analysis shows that selective dissolution of elements in the HEA is not evident compared to 304 L stainless steel during passivation. The passive film formed on the HEA is enriched in Fe and Mn but depleted in Cr. The low content of Cr and the extensive formation of metal hydroxide in the passive film are responsible for the lower anti-corrosion performance of the HEA. H. Feng et al. [29] investigated the corrosion behavior of the nitrogen-doped CrCoNiN in 3.5 wt.% NaCl solution. It was found that the nitrogen existed in the form of Cr2N precipitates and uniformly distributed N atoms, and nitrogen alloying significantly refined the grain size. The significantly improved corrosion resistance of CrCoNiN was attributed to the lower metastable pitting susceptibility and thicker, less defective, and more compact passive film. H. Gerengi et al. [5] investigated the corrosion behavior of aluminum 6060 and 6082 alloys by dynamic electrochemical impedance spectroscopy (DEIS) after exposure to simulated acid rain for 1, 5, 24, and 48 h. The results showed that DEIS is a sensitive technique detecting even very moderate changes in charge-transfer resistance; it exhibits an excellent correlation with surface morphological changes in relation to the exposure time. W. Q. Zhou et al. [9] studied the corrosion behavior of AZ91 magnesium alloy in simulating acid rain under wet-dry cyclic conditions. The results show that corrosion potential shifts positively, and the corrosion current density decreases at low wet-dry cyclic time. Further increase of the cyclic time results in the negative movement of corrosion potential and increased current density. SEM observation indicates that corrosion occurs only in the $\alpha$ phase, the $\beta$ phase is inert in the corrosive medium, and the corrosion of AZ91 magnesium appears in uniform characteristics. XPS analysis suggests that the corrosion product is mainly composed of oxide and hydroxide of magnesium and aluminum, and a small amount of sulfate is also contained in the film. A. K. Al-Harbi et al. [8] investigated the electrochemical behavior of two Metal-Metal glassy alloys $Fe_{78}Co_9Cr_{10}Mo_2Al1$ (VX9) and $Fe_{49}Co_{49}V_2$ (VX50) (at.%) at different immersion times in artificial acid rain using electrochemical techniques. VX9 alloy has higher corrosion resistance than VX50 due to good protective elements such as Cr 10% that create chromium oxide. Immersion measurements during (0.5–12 h) reveal the critical time for VX9 alloy is about 3 h to begin corrosion resistance, while the VX50 alloy takes longer to form a protective film. K. M. Saurabh et al. [33] investigated the effect of acid rain on the polished surface of as-cast Al6061 alloy through a simulated acid rain environment. The effect of surface roughness on the corrosion rate was also investigated. It was observed that the corrosion rate decreases as the surface finish of the specimen increases.

The excellent corrosion resistance of the HEA is a very critical factor affecting its service life for long--term engineering applications. In this study, Al was added to design and prepare equimolar CoCrNiAl HEA to improve the corrosion resistance of the alloy.

The method of investigating the harm degree of acid rain to materials usually adopts the full outdoor exposure test, but this mode requires a long time. Therefore, this study uses artificial simulated acid rain to accelerate electrochemical corrosion. The advantage is that the qualitative and quantitative results of various materials simulating the impact of acid rain corrosion in outdoor atmospheric environments can be obtained quickly. Furthermore, studying the electrochemical corrosion behavior of metals in simulated acid rain solution will provide a basis for taking appropriate measures to reduce the corrosion rate. The available research is to study the corrosion of typical metals such as carbon steel, copper, aluminum, and zinc in acid rain. In this study, the prepared CoCrNiAl HEA was placed in a simulated acid rain solution to study the corrosion behavior of the alloy in the simulated acid rain environment and lay a foundation for the practical application of the alloy, especially under specific conditions.

## 2. Experimental

The experimental flow chart is shown in Fig. 1. High purity (> 99.5 %) Co, Cr, Ni, and Al powders were used as powder materials. The CoCrNiAl HEA was prepared by vacuum arc melting and suction casting system (DHL300); the total mass of each alloy ingot is 45 g. Considering the different melting points of metals, they were placed so that the melting point decreased from top to bottom. When the vacuum degree reached $4.5 \times 10^{-3}$ Pa, high-purity argon was introduced to ensure that the alloy would not be oxidized and reduce element burning loss during smelting. During smelting, the alloy liquid was thoroughly stirred through induction magnetism. The alloy ingot was repeatedly melted 5 times to ensure uniformity. The obtained button ingot alloy was suction cast into a sheet with a thickness of 3 mm by the suction casting device. The microstructure of the HEA was observed by a metallographic microscope (9XF). The phase structure of the alloy was confirmed using X-ray diffraction (XRD-6000) measurement with a Cu target, the tube voltage was 40 kV, and the current was 45 mA. The range of diffraction scanning angle was 20°–90°, and the scanning speed was $5° \text{ min}^{-1}$.

To study the corrosion behavior of different metals under simulated acid rain, the widely used typical

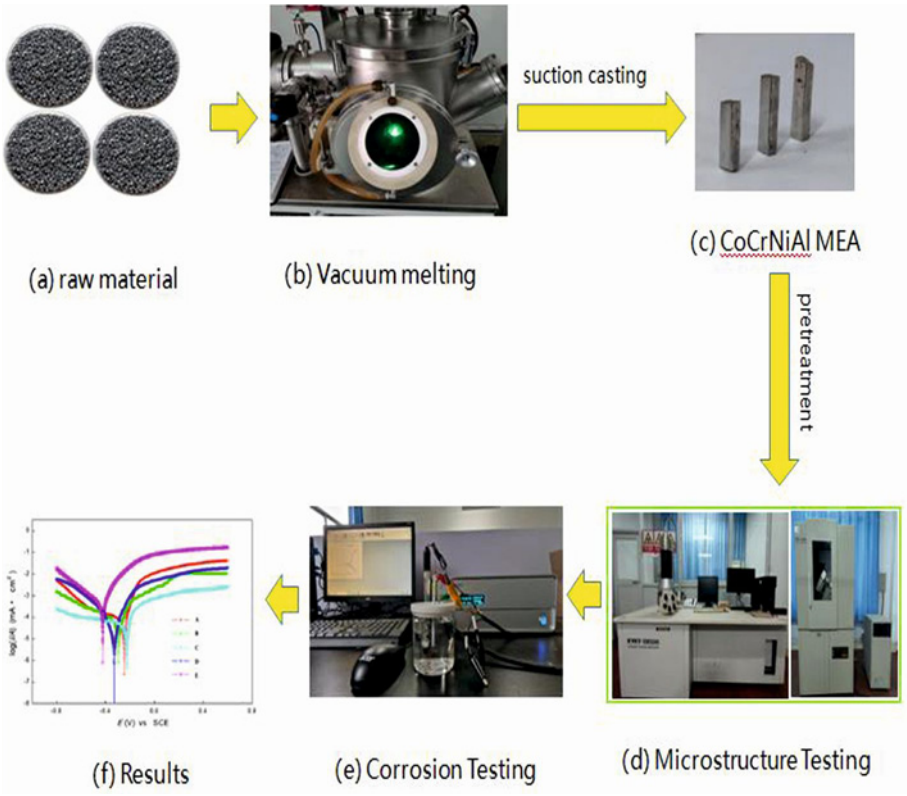


Fig. 1. Experimental flow chart.

Table 1. Chemical composition of Q235 steel

| C | Si | Mn | P | S | Cr | Ni | Fe |
|---|---|---|---|---|---|---|---|
| 0.22 | 0.35 | 1.40 | $\leq 0.045$ | $\leq 0.05$ | 0.01 | 0.01 | balance |

Table 2. Chemical composition of AZ31 magnesium alloy

| Fe | Si | Zn | Mn | Al | Cu | Ni | Mg |
|---|---|---|---|---|---|---|---|
| 0.003 | 0.16 | 0.61 | 0.32 | 3.05 | 0.006 | 0.001 | balance |

Table 3. Chemical composition of 1060 aluminum alloy

| Fe | Si | Zn | Mn | Cu | Mg | Ti | Al |
|---|---|---|---|---|---|---|---|
| 0.15 | 0.13 | 0.02 | 0.01 | 0.03 | 0.01 | 0.01 | balance |

metals Q235 steel, AZ31 magnesium alloy, and 1060 aluminum alloy were selected for comparison. The composition of the three typical metals is shown in Tables 1–3. The thickness of the three metal samples is 2 mm. Before the experiment, all samples were polished with SiC sandpaper, washed with acetone and distilled water, dried, and stored in a dryer. CoCrNiAl HEA suction cast samples used for microstructure observation were polished and corroded with aqua regia. All samples used for the electrochemical test were coated with epoxy resin to expose one side as the working surface; the effective working area of the research electrode is 1 $cm^2$. A scanning electron microscope (KYKY-EM3200) was used to observe the corrosion morphology of CoCrNiAl HEA, and the composition of the corrosion product was measured by the energy dispersive spectrometer (EDS) attached to it.

Table 4. Composition of simulated acid rain (mg $L^{-1}$)

| $SO_4^{2-}$ | $NO_3^-$ | $Ca^{2+}$ | $NH_4^+$ | $Mg^{2+}$ | $Cl^-$ | $K^+$ | $Na^+$ | $F^-$ |
|---|---|---|---|---|---|---|---|---|
| 20.5 | 4.7 | 5.4 | 3.0 | 0.4 | 1.8 | 1.0 | 0.5 | 0.4 |

The simulated rainwater was prepared with distilled water and pure analytical reagent according to the analysis results of the actual rainfall components in Sichuan Province; the composition is shown in Table 4. According to the national standard of the People's Republic of China *Specifications for acid rain monitoring* (GB/T 19117-2017), the acidity of simulated acid rain solution with sulfuric acid was adjusted to make pH = 3.5, 4.0, 4.5, and 5.0, respectively.

The polarization curves and cyclic polarization curves of samples in simulated rainwater with pH = 3.5, 4.0, 4.5, and 5.0 were measured by an electro-

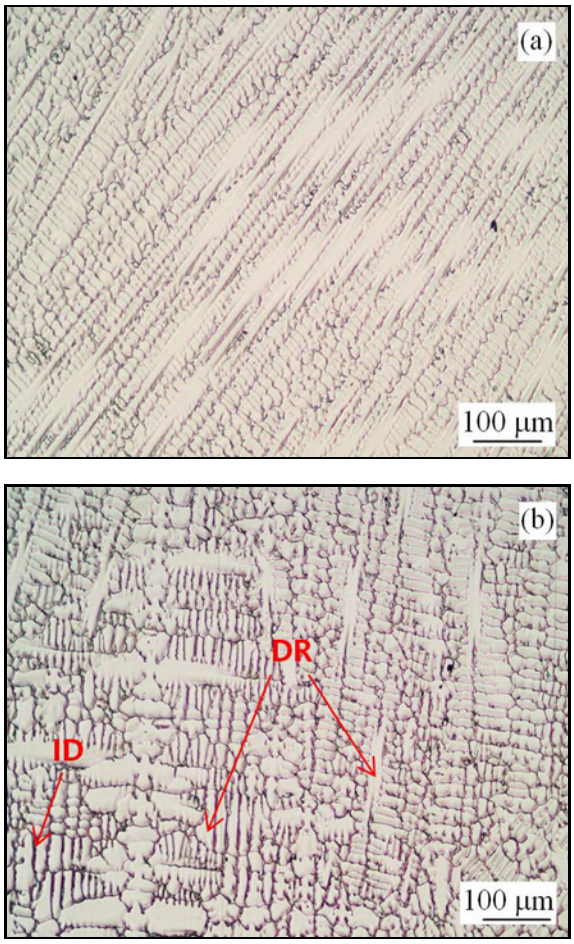


Fig. 2. Microstructure of CoCrNiAl HEAs.

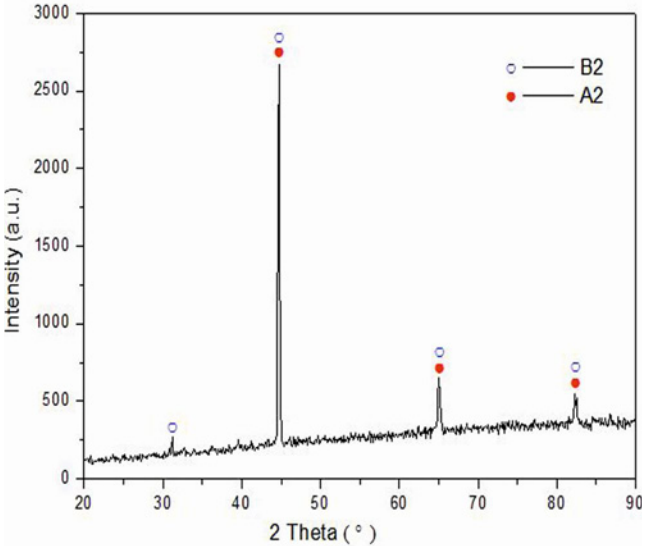


Fig. 3. XRD pattern of CoCrNiAl HEA.

Table 5. Chemical composition of the dendritic and the interdendritic regions of the AlCoCrNi HEA (at.%)

| Region | Al | Co | Cr | Ni |
|---|---|---|---|---|
| Dendrite | 27.6 | 24.2 | 19.6 | 28.6 |
| Interdendrite | 16.8 | 28.7 | 33.1 | 21.4 |

chemical workstation (CS310M) at room temperature. The three-electrode system was adopted: the reference electrode was a saturated calomel electrode, the auxiliary electrode was a platinum electrode, and the working electrode was a metal sample. The sample was placed in the solution for 20 min and tested until it was stable; the scanning speed was 1 mV $s^{-1}$.

## 3. Results and discussion

### *3.1. Microstructure and XRD*

The microstructure of the CoCrNiAl HEA is mainly composed of dendrites, as shown in Fig. 2, which are closely arranged. Dendrite is a kind of crystal that can retain its branches at a particular stage in the growth process. The dendrite growth process first forms the main branch and then divides the secondary branch on it until the branches at all levels are connected and joined with each other. If the supply of mother liquor is interrupted in the process, different forms of dendrites can be obtained directly. In addition, due to the different growth order of all dendrites, the metal dendrites can be displayed by erosion with an appropriate solution. The long-axis direction of the main branch is primarily consistent with a specific crystal direction.

To analyze the phase structure of the prepared CoCrNiAl HEA, an XRD test was performed, and the results are shown in Fig. 3. The CoCrNiAl alloy exhibits the diffraction patterns of the disordered A2-bcc phase with the ordered B2-bcc phase. The microstructural features, i.e., the formation of the A2/B2 dual-phase structure, have also been identified in the AlCoFeCrNi alloy [30–33]. The cross-sectional micrograph of the prepared AlCoCrNi HEA in Fig. 1b reveals a typical microstructure of dual-phase HEAs consisting of dendrites and interdendritic regions. The chemical composition of both regions measured by EDS is listed in Table 5.

The DR region exhibits a higher concentration of Al and Ni and a lower amount of Cr than the ID region, which indicates that the solute segregation into the Ni-Al-rich and Cr-rich regions occurred during the dendritic solidification. The segregation of the Cr content during the solidification has also been reported in other studies on AlCoCrFeNi alloy [31,

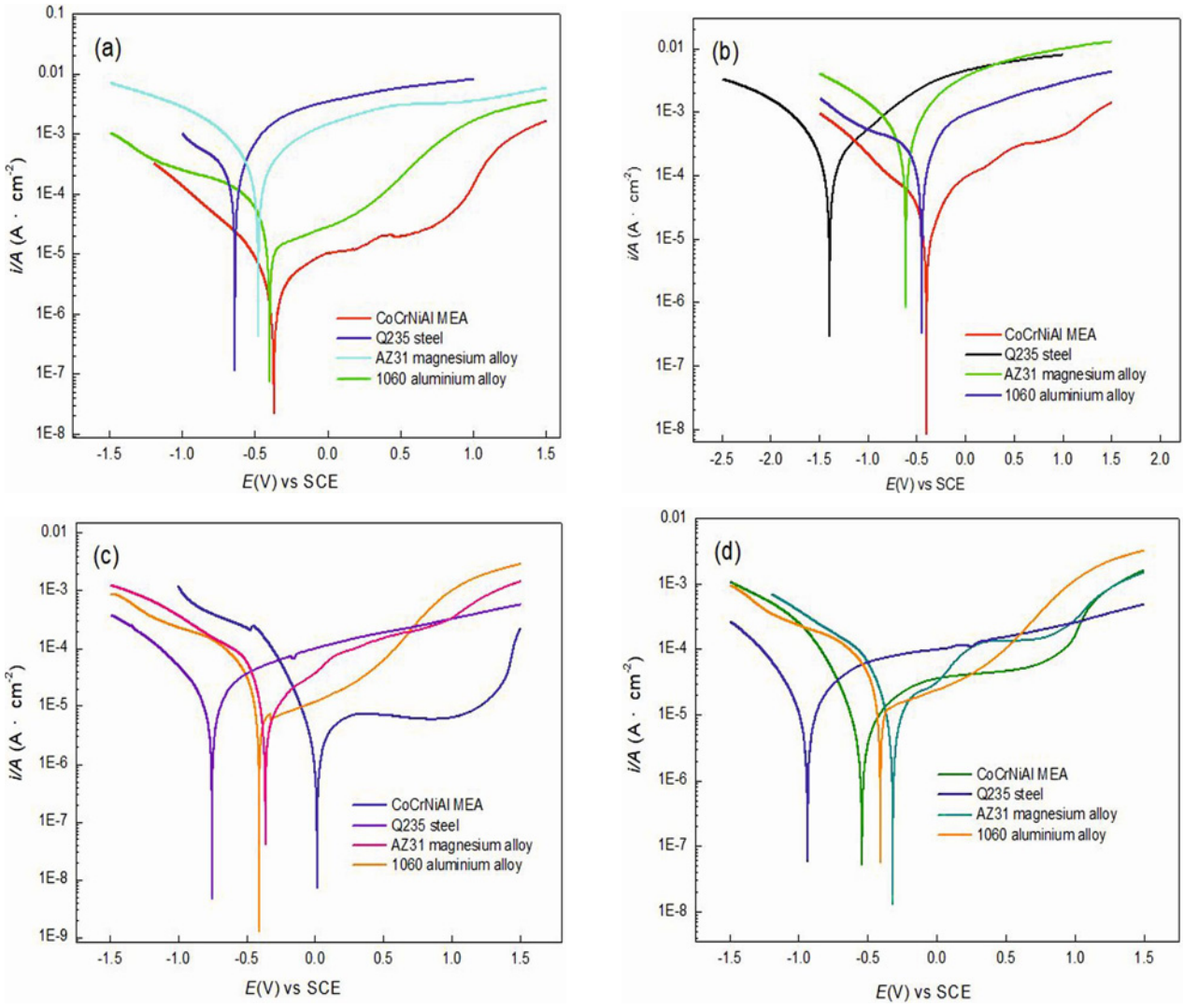


Fig. 4. Polarization curves of CoCrNiAl HEAs and other typical metals in simulated acid rain solutions (a) pH = 3.5, (b) pH = 4.0, (c) pH = 4.5, and (d) pH = 5.0.

Table 6. Corrosion dynamics parameters of CoCrNiAl HEA and other typical metals in simulated acid rain solutions

| Samples | pH = 3.5 | | pH = 4.0 | | pH = 4.5 | | pH = 5.0 | |
|---|---|---|---|---|---|---|---|---|
| | $E_{corr}$ (V) | $I_{corr}$ (A cm$^{-2}$) | $E_{corr}$ (V) | $I_{corr}$ (A cm$^{-2}$) | $E_{corr}$ (V) | $I_{corr}$ (A cm$^{-2}$) | $E_{corr}$ (V) | $I_{corr}$ (A cm$^{-2}$) |
| CoCrNiAl HEA | –0.39 | $7.5 \times 10^{-7}$ | –0.46 | $7.8 \times 10^{-6}$ | 0.01 | $6.1 \times 10^{-7}$ | –0.52 | $9.5 \times 10^{-7}$ |
| Q235 steel | –0.61 | $6.9 \times 10^{-5}$ | –1.45 | $5.8 \times 10^{-5}$ | –0.77 | $3.9 \times 10^{-6}$ | –0.97 | $1.4 \times 10^{-6}$ |
| AZ31 magnesium alloy | –0.49 | $6.8 \times 10^{-5}$ | –0.56 | $6.6 \times 10^{-5}$ | –0.43 | $4.0 \times 10^{-6}$ | –0.41 | $1.5 \times 10^{-6}$ |
| 1060 aluminum alloy | –0.42 | $7.3 \times 10^{-6}$ | –0.49 | $6.2 \times 10^{-5}$ | –0.46 | $4.2 \times 10^{-6}$ | –0.46 | $7.3 \times 10^{-6}$ |

32]. Based on these results, it is confirmed that the AlCoCrNi HEA designed by excluding the Fe content from the AlCoCrFeNi alloy solidifies into the Ni-Al rich DR and Cr-rich ID regions that consist of the A2/B2 dual-phase structure, which is very similar to the microstructural morphologies of the AlCoCrFeNi alloy.

### *3.2. Electrochemical performance*

Figure 4 shows the polarization curves of CoCrNiAl HEA and other typical metals in simulated acid rain solutions with pH = 3.5, 4.0, 4.5, and 5.0.

Table 6 illustrates the corrosion kinetic parameters obtained by linear fitting. Combined with Fig. 4 and

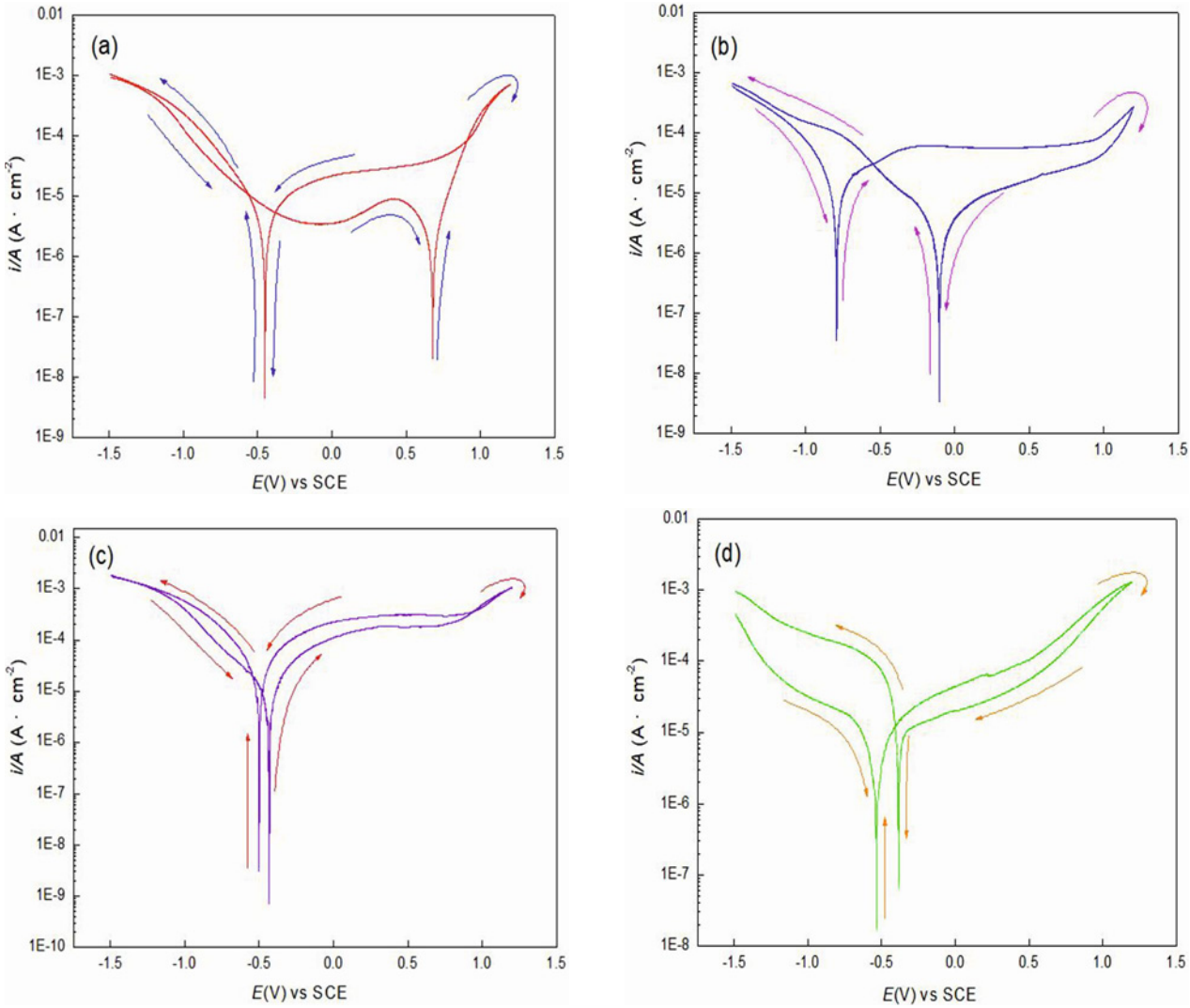


Fig. 5. Circular polarization curve of CoCrNiAl HEAs in simulated acid rain solutions: (a) pH = 3.5, (b) pH = 4.0, (c) pH = 4.5, and (d) pH = 5.0.

Table 6, the self-corrosion current of CoCrNiAl HEA is lower than that of Q235 steel, AZ31 magnesium alloy, and 1060 aluminum alloy, with a reduced range of 1–2 orders of magnitude. The self-corrosion potential is positive except in a solution with pH = 5.0. According to electrochemical theory, the self-corrosion current is the main factor affecting corrosion resistance, followed by self-corrosion potential. The smaller the self-corrosion current, the higher the self-corrosion potential and the better the corrosion resistance.

Although the self-potential of CoCrNiAl alloy is lower than that of AZ31 magnesium alloy and 1060 aluminum alloy in simulated acid rain solution with pH = 5.0, the self-corrosion current is two orders of magnitude lower. Co and Ni elements in CoCrNiAl alloy coating have excellent corrosion resistance, which is easy to passivate to improve corrosion resistance. The dense dendrite structure of the alloy also provides a guarantee for excellent corrosion resistance.

With the increase in pH, the self-corrosion current of Q235 steel decreases gradually, because the cathodic process of Q235 steel corrosion in simulated acid rain solution is mainly the depolarization reaction of $H^+$ and $O_2$. Under the condition of low pH, $H^+$ concentration plays a decisive role in the corrosion rate of steel. With the increase of acidity, the cathodic reaction rate dominated by $H^+$ reduction increases, which enhances the dissolution of steel and the corrosion rate.

With the increase in pH, the self-corrosion current of an AZ31 magnesium alloy becomes smaller. Under the same corrosion potential, the anode polarization current density increases with the decrease in pH, and the corrosion rate increases. The change in pH has a significant impact on the anode process. This is because the anodic reaction of magnesium alloy in a simulated acid rain solution is the dissolution process of magnesium. The pH of the solution decreases, the

corresponding hydrogen equilibrium potential moves forward, the thermodynamic trend of corrosion reaction increases, and the dissolution rate of magnesium increases.

Aluminum is a relatively active metal, which is easily oxidized in the air to form a dense and solid oxide film ($Al_2O_3$). The corrosion resistance of aluminum alloy depends on the integrity and self-healing ability of this oxide film. Ions in the simulated solution, such as $Cl^-$, $SO_4^{2-}$, $H^+$, and dissolved oxygen, are competitively adsorbed on the oxide film, and the adsorption mainly occurs at the defects of the oxide film, which forms a pitting source of local corrosion. The adsorbed ions react with the oxide film, thinning the local oxide film, exposing the active aluminum matrix, and dissolving to produce aluminum ions. Aluminum and adsorbed ions form intermediate products, which separate from the matrix and enter the solution or form stable corrosion products and deposit on the surface of the matrix. In the acidic environment, the oxide film dissolves and thins due to the interaction of $H^+$ in the solution, resulting in more pitting sources on the surface. At the same time, it reduces the resistance of ions and electrons adsorbed on the surface to pass through the oxide film, accelerates the erosion of active anions to the matrix, and accelerates the dissolution of aluminum alloy.

To evaluate the uniformity of CoCrNiAl alloy, the pitting corrosion resistance in simulated acid rain solution with different pH was tested by cyclic polarization curve; Fig. 5 shows the results.

It is generally believed that the presence of a positive hysteresis loop on the cyclic polarization curve indicates that pitting corrosion is easy to occur, and the absence of a hysteresis loop or negative hysteresis loop on the cyclic polarization curve indicates that pitting corrosion will not occur.

Negative hysteresis loops appear in all cyclic polarization curves, indicating that CoCrNiAl alloy is uniform and resistant to pitting corrosion. Due to the existence of Al in the alloy, it is easy to form a passive film on the alloy surface, which plays a protective role. According to the corrosion parameters in Table 6, the corrosion current is relatively low. Therefore, it has excellent pitting corrosion resistance.

The corrosion mechanism of the prepared CoCrNiAl alloy is intergranular corrosion when it comes into contact with a simulated acid rain solution. Local corrosion occurs because the dissolution rate of the grain boundary components in the metal in the medium is much higher than that of the grain body. Due to the high energy at the grain boundary, the atoms are unstable, and the impurity atoms are enriched at the grain boundary; the corrosion rate at this position is faster. With the extension of time, the alloy surface gradually appears to have extensive corrosion, and the corrosion mechanism changes to uniform corrosion. Comparing Fig. 6a with Fig. 6b, it can be seen that the corrosion degree is more serious when pH = 4.0, mainly because the sulfate ion concentration in the simulated acid rain solution is higher after corrosion, little remains of the original grain boundary (OGB), that is, the black part and the corrode grain boundary (CGB) is still faintly visible. With the further extension of time, since the prepared simulated acid rain solution adopts $H_2SO_4$ to adjust the pH, the easily passivated metal can quickly generate corrosion products (CP) on the surface of the sample, thus slowing down the corrosion rate and playing a specific protective role. As shown in Fig. 6, the prepared CoCrNiAl HEAs generate sulfate and oxides such as $MSO_4$ and $M_2O$ on the alloy surface in the simulated acid rain solution, and the corrosion products adhere to the alloy surface tightly to protect the internal alloy and slow down the corrosion of the alloy surface. EDS analysis is carried out on the corrosion products. The results are shown in Table 7. The analysis shows that the corrosion products mainly contain O and S, indicating the formation of sulfate and oxide.

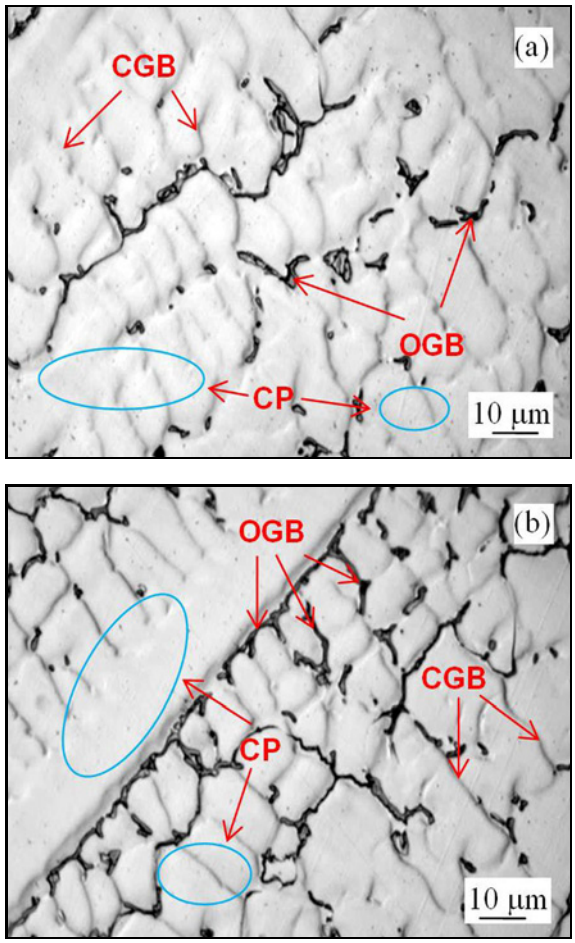


Fig. 6. Surface corrosion morphology of CoCrNiAl HEAs in simulated acid rain solutions (a) pH = 4.0 and (b) pH = 5.0.

Table 7. Energy Disperse Spectroscopy (EDS) of the AlCoCrNi HEA in simulated acid rain solutions (a) pH = 4.0 and (b) pH = 5.0 (at.%)

| pH | Al | Co | Cr | Ni | O | S |
|---|---|---|---|---|---|---|
| 4.0 | 4.9 | 6.3 | 7.2 | 8.6 | 60.2 | 12.8 |
| 5.0 | 3.8 | 8.7 | 9.4 | 9.8 | 57.6 | 10.7 |

## 4. Conclusions

This study investigated the corrosion behavior of CoCrNiAl HEA under simulated acid rain conditions and compared it with other typical metals. The following conclusions can be drawn from the results herein:

1. The microstructure of CoCrNiAl HEA is mainly composed of dendrites. The CoCrNiAl alloy comprises disordered BCC (A2) and ordered BCC (B2) phases.

2. The CoCrNiAl HEA has excellent corrosion resistance in simulated acid rain solution with pH = 3.5, 4.0, 4.5, and 5.0. The self-corrosion current is reduced by 1–2 orders of magnitude compared with Q235 steel, AZ31 magnesium alloy, and 1060 aluminum alloy. The self-corrosion potential is improved except in simulated acid rain solution with pH = 5. Negative hysteresis loops appear in the cyclic polarization curves, showing that the CoCrNiAl HEA has excellent pitting corrosion resistance in a simulated acid rain environment.

3. The corrosion resistance of CoCrNiAl HEA is related to the uniformity and compactness of microstructure, passive film, corrosion-resistant elements, and dense corrosion products.

4. With the extension of time, the corrosion mechanism of the CoCrNiAl alloy in the simulated acid rain solution was changed from the initial intergranular corrosion to the uniform corrosion.

## Acknowledgements

This work was supported by Natural Science Foundation of Sichuan Province (2023NSFSC0406), Key R & D Projects of Deyang Science and Technology Plan, Sichuan Province, China (2021SZ009), Scientific Research and Innovation Team Foundation of Sichuan College of Architecture Technology (SCJYKYCXTD 2022), and the Research Project of Sichuan College of Architecture Technology (2022KJ01).

## References

[1] R. Liu, L. Liu, F. H. Wang, The role of hydrostatic pressure on the metal corrosion in simulated deep-sea environments – a review, J. Mater. Sci. Technol. 112 (2022) 230–238. https://doi.org/10.1016/j.jmst.2021.10.014

[2] L. Jiang, Y. M. Dong, Y. Yuan, X. Zhou, Y. R. Liu, X. K. Meng, Recent advances of metal-organic frameworks in corrosion protection: From synthesis to applications, Chem. Eng. J. 430 (2022) 132823. https://doi.org/10.1016/j.cej.2021.132823

[3] J. Y. Liu, D. M. Chen, B. Su, D. H. Chen, Z. Y. Ren, D. L. Zou, K. Z. Liu, Effects of ultrasonic surface rolling processing on the corrosion properties of uranium metal, J. Nucl. Mater. 556 (2021) 153239. https://doi.org/ 10.1016/j.jnucmat.2021.153239

[4] F. Liu, Y. W. Song, D. Y. Shan, E. H. Han, Corrosion behavior of AZ31 magnesium alloy in simulated acid rain solution, Trans. Nonferrous Met. Soc. China 15 (2010) 638–642. https://doi.org/10.1016/j.jmrt.2021.09.078

[5] H. Gerengi, G. Bereket, M. Kurtay, A morphological and electrochemical comparison of the corrosion process of aluminum alloys under simulated acid rain conditions, J. Taiwan Inst. Chem. E. 58 (2016) 509–516. https://doi.org/10.1016/j.jtice.2015.05.023

[6] L. J. Yang, Y. M. Zhang, X. D. Zeng, Z. L. Song, Corrosion behaviour of superplastic Zn–Al alloys in simulated acid rain, Corros. Sci. 59 (2012) 229–237. https://doi.org/10.1016/S1003-6326(10)60553-5

[7] Y. Y. Shi, Z. Zhang, J. X. Su, F. H. Cao, J. Q. Zhang, Electrochemical noise study on 2024-T3 Aluminum alloy corrosion in simulated acid rain under cyclic wet-dry condition, Electrochim. Acta 51 (2006) 4977–4986. https://doi.org/10.1016/j.electacta.2006.01.050

[8] A. K. Al-Harbi, K. M. Emran, Effect of immersion time on electrochemical and morphology of new Fe-Co metal-metal glassy alloys in acid rain, Arab. J. Chem. 12 (2019) 134–141. https://doi.org/10.1016/j.arabjc.2018.01.019

[9] W. Q. Zhou, D. Y. Shan, E. H. Han, W. Ke, Initial corrosion behavior of AZ91 magnesium alloy in simulating acid rain under wet-dry cyclic condition, Trans. Nonferrous Met. Soc. China 18 (2008) 334–338. https://doi.org/10.1016/S1003-6326(10)60227-0

[10] Y. Murakami, Y. Maeda, A. Kitada, K. Murase, K. Fukami, Electrodeposition of a CoNiCu medium-entropy alloy in a water-in-oil emulsion, Electrochem. Commun. 128 (2021) 107057. https://doi.org/ 10.1016/j.elecom.2021.107057

[11] X. Xu, C. H. Wang, J. W. Zou, C. J. Zhang, Y. Z. Chen, Y. K. Du, X. C. Ma, Z. Zeng, L. Q. Li, Nickel-rich NiCeLaFeCo medium-entropy alloy nanoparticles on oxygen and nitrogen co-doped carbon supports for hydrogen production from toluene cracking, J. Alloy. Compd. 903 (2022) 163935. https://doi.org/10.1016/j.jallcom.2022.163935

[12] J. J. Wang, F. Y. Ouyang, Nanotwinned high entropy alloy CoCrFeNi thin films with ultra-high hardness: Modifying residual stress without scarifying hardness through tuning substrate bias, Surf. Coat. Tech. 434 (2022) 128191. https://doi.org/10.1016/j.surfcoat.2022.128191

[13] P. K. Shen, H. C. Liu, C. Y. Huang, H. W. Yen, J. W. Yeh, C. W. Tsai, Microstructure and mechanical properties of medium-entropy alloys with a high-density $\eta$-$D_{024}$ phase, Mater. Charact. 185 (2022) 111713. https://doi.org/10.1016/j.matchar.2021.111713

[14] Q. Q. Zhu, G. R. Xiao, Y. W. Cui, W. Z. Yang, S. Q. Wu, G. H. Cao, Z. Ren, Structural transformation of MoReRu medium-entropy alloy by carbon addition, Scripta Mater. 210 (2022) 114464. https://doi.org/10.1016/ j.scriptamat.2021.114464
[15] H. Y. Xin, J. J. Yang, W. Zhang, J. Yang, J. J. Mao, C. Q. Teng, X. G. Kong, J. X. Si, X. Y. Xu, W. Zhang, L. Wu, X. Y. Wu, Effect of Au ion irradiation on the surface morphology, microstructure and mechanical properties of AlNbTiZr medium-entropy alloy coatings with various Al content for ATF, Surf. Coat. Tech. 434 (2022) 128157. https://doi.org/ 10.1016/j.surfcoat.2022.128157
[16] C. C. Wang, S. J. Lin, S. Y. Chang, Y. C. Lo, J. F. Chen, Y. C. Chuang, T. N. Lam, H. S. Sheu, E. W. Huang, Thermal effects on stability of hierarchical microstructure in medium- and high-entropy alloys, Mater. Chem. Phys. 278 (2022) 125677. https://doi.org/10.1016/j.matchemphys.2021.125677
[17] Q. Y. Zhou, S.Sheikh, P. Ou, D. C. Chen, Q. Hu, S. Guo, Corrosion behavior of $Hf_{0.5}Nb_{0.5}Ta_{0.5}Ti_{1.5}Zr$ refractory high-entropy in aqueous chloride solutions, Electrochem. Commun. 98 (2019) 63–68. https://doi.org/10.1016/j.elecom.2018.11.009
[18] J. C. Zhang, T. W. Huang, Z. L. Shen, H. J. Su, J. Zhang, L. Liu, Enhanced structural refinement on eutectic medium-entropy alloy $CrCoNiNb_{0.48}$ by laser remelting, Mater. Lett. 304 (2021) 130710. https://doi.org/10.1016/j.matlet.2021.130710
[19] Q. S. Wang, A. Sarkar, Z. Y. Li, Y. Lu, L. Velasco, S. S. Bhattacharya, T. Brezesinski, H. Hahn, B. Breitung, High entropy oxides as anode material for Li-ion battery applications: A practical approach, Electrochem. Commun. 100 (2019) 121–125. https://doi.org/10.1016/j.elecom.2019.02.001
[20] W. Kai, Z. Y. Jiang, G. T. Chen, I. H. Lee, H. J. Lin, H. H. Hsieh, W. T. Lin, J. J. Kai, High-temperature air-oxidation of $NiCoCrAl_x$ medium-entropy alloys, Corros. Sci. 192 (2021) 109858. https://doi.org/10.1016/j.corsci.2021.109858
[21] D. C. Zhao, D. C. Kong, J. Huang, M. L. Wang, T. Yamaguchi, H. W. Wang, Achieving the lightweight wear-resistant TiC reinforced AlFeCrCo medium-entropy alloy coating on Mg alloy via resistance seam processing, Scripta Mater. 210 (2022) 114429. https://doi.org/10.1016/j.scriptamat.2021.114429
[22] F. Sun, G. Miyamoto, Y. K. Liu, Y. Hayasaka, T. Furuhara, Phase separation with ordering in aged Fe-Ni-Mn high entropy alloy, Acta Mater. 223 (2022) 117487. https://doi.org/10.1016/j.actamat.2021.117487
[23] J. Yi, X. Q. Zhuang, J. He, M. L. He, W. H. Liu, S. Wang, Effect of Mo doping on the gaseous hydrogen embrittlement of a CoCrNi medium-entropy alloy, Corros. Sci. 189 (2021) 109628. https://doi.org/10.1016/j.corsci.2021.109628
[24] L. Zhang, Z. H. Hu, L. Zhang, H. Wang, J. B. Li, Z. Li, J. X. Yu, B. L. Wu, Enhancing the strength-ductility trade-off in a NiCoCr-based medium-entropy alloy with the synergetic effect of ultra fine precipitates, stacking faults, dislocation locks and twins, Scripta Mater. 211 (2022) 114497. https://doi.org/10.1016/j.scriptamat.2021.114497
[25] S. W. Hu, T. J. Li, Z. Q. Su, D. X. Liu, Research on suitable strength, elastic modulus and abrasion resistance of Ti-Zr-Nb high entropy alloys (HEAs) for implant adaptation, Intermetallics 140 (2022) 107401. https://doi.org/10.1016/j.intermet.2021.107401
[26] S. R. Huang, H. Wu, H. G. Zhu, Z. H. Xie, In-situ $TiC/Fe_{0.6}MnNi_{1.4}$ medium entropy alloy matrix composites with excellent strength-ductility synergy, Ceram. Int. 47 (2021) 26319–26326. https://doi.org/10.1016/j.ceramint.2021.06.042
[27] B. Gludovatz, A. Hohenwarter, K. V. S. Thurston, H. B. Bei, Z. G. Wu, E. P. George, R. O. Ritchie, Exceptional damage-tolerance of a medium-entropy alloy CrCoNi at cryogenic temperatures, Nat. Commun. 7 (2016) 10602. https://doi.org/10.1038/ncomms10602
[28] H. Luo, Z. M. Li, A. M. Mingers, D. Raabe, Corrosion behavior of an equiatomic CoCrFeMnNi high-entropy alloy compared with 304 stainless steel in sulfuric acid solution, Corros. Sci. 134 (2018) 131–139. https://doi.org/10.1016/j.corsci.2018.02.031
[29] H. Feng, H. B. Li, X. L. Wu, Z. H. Jiang, S. Zhao, T. Zhang, D. K. Xu, S. C. Zhang, H. C. Zhu, B. B. Zhang, M. X. Yang, Effect of nitrogen on corrosion behaviour of a novel high nitrogen medium-entropy alloy CrCoNiN manufactured by pressurized metallurgy, J. Mater. Sci. Technol. 34 (2018) 1781–1790. https://doi.org/10.1016/j.jmst.2018.03.021
[30] K. M. Saurabh, C. Prashant, P. Rabindra, K. S. Chander, M. Alakesh, Effect of surface finish on corrosion behavior of polished Al6061 alloy in simulated acid rain environment, Mater. Today Proc. 64 (2022) 755–759. https://doi.org/10.1016/j.matpr.2022.05.208
[31] A. Manzoni, H. Daoud, R. Völkl, U. Glatzel, N. Wanderka, Phase separation in equiatomic AlCoCrFeNi high-entropy alloy, Ultramicroscopy 132 (2013) 212–215. https://doi.org/10.1016/j.ultramic.2012.12.015
[32] K. R. Lim, K. S. Lee, J. S. Lee, J. Y. Kim, H. J. Chang, Y. S. Na, Dual-phase high entropy alloys for high-temperature structural applications, J. Alloy. Compd. 728 (2017) 1235–1238. https://doi.org/10.1016/j.jallcom.2017.09.089
[33] S. Antonov, M. Detrois, S. Tin, Design of novel precipitate-strengthened Al-Co-Cr-Fe-Nb-Ni high-entropy superalloys, Metall. Mater. Trans. A 49 (2018) 305–320. https://doi.org/10.1007/s11661-017-4399-9